I.A.U
Karaj branch

Journal of
A p p l ied
C hemical
R esearch
jacr.kiau.ac.ir

Journal of Applied Chemical Research, 16, 2, 72-85 (2022)

Electrochemical Determination of Dopamine Based on Magnetic Molecularly Imprinted Nanocomposite and Ionic Liquid Functionalized Carbon Paste Electrode in the Biological Samples

Farzaneh Shaker, Mohammad Taghi Vardini*, Moosa Es'haghi, Ebrahim GhorbaniKalhor

Department of Chemistry, Tabriz Branch, Islamic Azad University, Tabriz, Iran

(Received 19 Aug. 2021; Final revised received 09 Nov. 2021)

Abstract

Dopamine (DA) is a well-known neurotransmitter in the brain that is related to mental and motivational states. Therefore, its measurement is essential. A sensitive electrochemical molecularly imprinted sensor-based new nanocomposite was developed for the detection of DA. The structural basis of nanocomposite was composed of molecularly imprinted polymer (MIP) polymerization of methacrylic acid (MAA) in the presence of DA as a template molecule. The MIP was decorated with Fe_3O_4 particles, ionic liquid (IL), and gold nanoparticles (AuNPs). MIP modified nanocomposite was used as the main component of the carbon paste electrode (CPE). The morphology of the designed nanocomposite was studied by scanning electron microscope (SEM), and Fourier transforms infrared spectroscopy (FT-IR) techniques. The performance of the developed sensor was investigated by cyclic voltammetry (CV), and differential pulse voltammetry (DPV) techniques for the detection of DA. The MIP sensor exhibits a broad linear range, between 6×10^{-8} to 1×10^{-5} M, and a limit of detection of 1×10^{-10} M (S/N=3). Furthermore, the modified MIP sensor was successfully employed to test DA in urine and blood samples.

Keywords: Molecularly imprinted polymer, Magnetic graphene oxide, Gold nanoparticles, Electrochemical sensor.

***Corresponding author:** *Mohammad Taghi Vardini, Department of Chemistry, Tabriz Branch, Islamic Azad University, Tabriz, Iran. E-mail:* mtvardini@iaut.ac.ir, *P.O. Box 5157944533, Tel: +98 9141064177, Fax: +98 4113333458.*

Introduction

Neurotransmitters are often referred to as the body's chemical messengers. They are molecules used by the nervous system to transmit messages between neurons to muscles [1]. Most neurotransmitters are small amine molecules or amino acids and neuropeptides. One of the key neurotransmitters is DA[2]. DA plays an important role in coordinating motivational states and body movements. Parkinson's disease is caused by the loss of DA-producing neurons in the brain. This disease causes movement and nervous disorders [3]. Nowadays several methods such as high-performance liquid chromatography (HPLC)[4], gas chromatography-mass spectrometry (GC-MS) [5], electrophoresis[6], etc. are used to determine DA. Nevertheless, all these methods are expensive and time-consuming. Compared to these methods, electrochemical techniques are simple, sensitive, and low cost in terms of tools and personnel [7]. Therefore electrochemical techniques are used as common analytical methods for the detection of DA[8].

Recently carbon paste electrodes (CPEs) based on molecularly imprinted polymers (MIPs) are designed as an electrochemical sensor [9]. Electrochemical sensors based on MIPs have a high selectivity since MIP particles have specific detection locations that can be highly selective with the template species [10]. In addition, MIP electrochemical sensors have mechanical, thermal, and chemical stability in harsh environments. The electrochemical signal of the MIP sensor increased by magnetic particles has high electrical conductivity, non-toxicity, and catalytic activity [11]. Moreover, IL improves the kneading properties of the CPE structure, making it more stable [12]. AuNPs doped with composite matrix on the CPE structure increase the electron transfer efficiency [13]. Therefore, MIP electrochemical sensors have three electrodes that modified CPE as the working electrode, platinum as the auxiliary electrode, and Ag/AgCl, KCl as the reference electrode for the diagnosis and clinical identification of drugs as well as biochemical carriers including hormones and neurotransmitters[14].

Kaya et al. designed a novel MIP electrochemical sensor for sensitive and selective DA determination[15]. Ma's group fabricated a novel MIP electrochemical sensor based on a 3D multi-walled carbon nanotube for the determination of DA [16]. Zhao et al. prepared an electrochemical sensor based on MIP for the sensitive determination of DA [17]. These MIP sensors could be used for the electrochemical determination of DA, however, conductivity, and cohesion of MIPs modified electrodes are low because of the lack of graphene oxide, Fe_3O_4particles, IL, and AuNPs in sensors structure.

In the current work, a MIP electrochemical sensor based on Fe_3O_4-IL-AuNPs nanocomposite was designed to determine DA in biological samples. In this regard, graphene oxide (GO) was synthesized from graphite. Then Fe_3O_4 particles, IL, and AuNPs as the conductive factors were

synthesized surface of GO. Finally, after the synthesis of the modified nanocomposite, MIP was synthesized by ethylene glycol dimethacrylate (EGDMA) and MAA monomers in the presence of DA molecules. The CPE was composed of MIP modified nanocomposite as a working electrode. CV, DPV, and electrochemical impedance spectroscopy (EIS) examined the electrochemical properties of the designed sensor by modified MIP nanocomposite. To the best of the authors' knowledge, this is the first time that Fe_3O_4 particles, IL, and gold particles are grafted on the surface of GO for the preparation of MIPs. The MIP-prepared sensor with high selectivity and sensitivity was employed for DA detection in urine and blood samples.

Experimental

Materials and instruments

Very fine pure graphite powder, DA, and EGDMA were purchased from Sigma Aldrich (USA). IL (1-hexyl-3-methyl-imidazolium bromide), hydrochloric acid (HCl), concentrated sulphuric acid (H_2SO_4), sodium nitrate ($NaNO_3$), potassium permanganate ($KMnO_4$), hydrogen peroxide (H_2O_2), ferrous chloride ($FeCl_2$), ferric chloride ($FeCl_3$), chloroauric acid ($HAuCl_4$), potassium ferricyanide $K_4[Fe(CN)_6]$, tri-sodium citrate, acetonitrile, ethanol, MAA, azobisisobutyronitrile (AIBN), ammonium persulfate (APS) $(NH_4)_2S_2O_8$, ammonium nitrate (NH_4NO_3), ammonium chloride (NH_4Cl), potassium nitrate (KNO_3), potassium chloride (KCl), sodium chloride (NaCl), potassium hydroxide (KOH), barium hydroxide($Ba(OH)_2$), zinc sulfate ($ZnSO_4$), and paraffin were all obtained from Merck (Germany). All the chemicals were of high purity and all the aqueous solutions were prepared with double-distilled water. SEM studied the morphology of the nanocomposite. The structural properties of nanoparticles were studied by FT-IR spectra. Electrochemical measurements were developed by Autolab PGSTAT302N (Netherlands) based on the three-electrode system. The EIS data were obtained by a $[Fe(CN)_6^{-3/-4}]$ solution (frequency range: 0.1 to 10000 Hz; signal amplitude: 0.01 V).

Synthesis of GO-Fe_3O_4

GO was synthesized from pure and natural graphite powder using the Hummers' method [18]. To synthesize the Fe_3O_4 particles, first, 350 mg of $FeCl_2$, 500 mg of $FeCl_3$, and 50 mg of GO were added to 100 mL of distilled water. After half an hour of ultrasonic stirring, the pH of the suspension was set to 9 by APS solution and the temperature reached 90 °C. The suspension remained at this temperature for 1 hour. The particles were washed with a 100 mL 0.1 M NaCl solution and 50 mL of ethanol. The Fe_3O_4 particles were isolated in a magnetic field and the supernatant was separated and heated at 60 °C in the vacuum oven.

Synthesis of GO-Fe_3O_4-IL-AuNPs

The composite of GO-Fe_3O_4-IL was synthesized by160 mg of magnetic particles, 37 mg of IL, and 150 mL of distilled water and stirred at 50 °C. The remained solid particles after 5 h of stirring were separated and dried at 60 °C for 24 h. The AuNPs were synthesized by a reduction in tri-sodium citrate with a series of minor corrections. 3.65 mL of 0.1 M $HAuCl_4$ solution was dissolved in 150 mL of distilled water and heated under stirring until boiling. Then, 3 mL of tri-sodium citrate (1 wt%) was slowly added to the aqueous solution. Finally, when the color of the solution turned red, indicating the formation of AuNPs, heating was stopped and the solid particles were synthesized at room temperature (4 °C). All the Fe_3O_4-GO particles were added to 15 mL of the red solution of AuNPs and stirred vigorously for 2 hours until the solution became colorless. The solid particles were separated in a magnetic field and dried in a vacuum oven at 60 °C. Eventually, GO-Fe_3O_4-IL-AuNPswere formed.

Synthesis of GO-Fe_3O_4-IL-AuNPs@MIP

DA was used as the template, while MAA, EGDMA, and AIBN were employed as the functional monomer, the cross-linking monomer, and the initiator in the polymerization process, respectively. The polymer particles were synthesized with an optimal ratio of 1:2:20 (DA, MAA, and EGDMA, respectively). At first, 100 mg Fe_3O_4-GO-IL-AuNPs was added to 40 mL of distilled water, after 15 minutes ultrasonic, 0.2 mmol DA, 0.4 mmol functional monomers, 4 mmol cross-linker, and 150 mg of the initiator were added to the reaction mixture, and it was refluxed at 60 °C for 24 hours. The solid particles were washed with acetonitrile and separated by the magnetic field of a magnet. To remove the template molecules, the modified MIP particles formed were placed in 50 mL of HCl solution (0.1 M) for 6 hours under stirring. The final product was dried at 60 °C in a vacuum oven. The Fe_3O_4-GO-IL-AuNPs@NIP were synthesized by MIP synthesis procedure only not using the template molecule during the polymerization process.

Preparation of CPE

The structure of CPE by 100 mg of modified MIP nanocomposite, 40 mg graphite powder, and 60 mg paraffin oil was prepared. In this regard, these materials were mixed and a smooth and soft paste was obtained. The resulting paste was packed into the ends of slim tubes using copper wires with a diameter of 4 mm. After complete drying, the surface of the electrode was smoothed with sandpaper and rested in acetonitrile as a preparation solution for 1 hour.

Results and discussion

Characterization

SEM images were used to characterize the morphology of modified nanocomposite step by step (Figure 1).

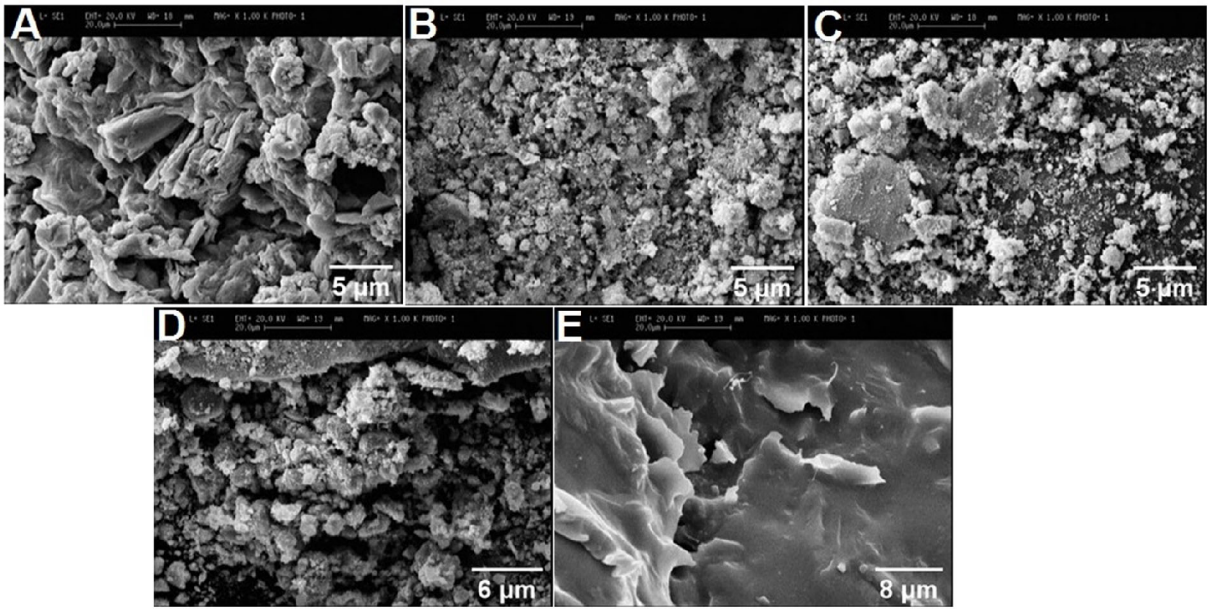

Figure 1. The types of SEM images from GO (A), MGO (B), MGO@IL (C), MGO@IL-AuNPs (D), and MGO@IL@AuNPs-MIP after removing DA(E).

GO is observed in Figure 1A as sheet-like structures with smooth and thick surfaces and some wrinkles. These wrinkles were very important for maintaining high levels of graphene oxide. Figure 1B shows that the Fe_3O_4 particles were dispersed on the GO plates. The size of the synthesized particles at this step was about 5 µm. Figure 1C shows the synthesized particles of GO-Fe_3O_4-IL. Figure 1D shows the actual size of the synthesized AuNPs, which are distributed over the surface compost regularly, was about 6 µm. Figure 1E shows the synthesized nanocomposite of GO-Fe_3O_4-IL@MIPafter removing DA. In this figure, the wrinkles are not visible because polymer layers are placed on nanocomposite surfaces. The size of the synthesized particles at this stage was about 8 µm.

FT-IR spectra

To further investigate the structure of the modified nanocomposite, the FT-IR spectrum was used (Figure 2).

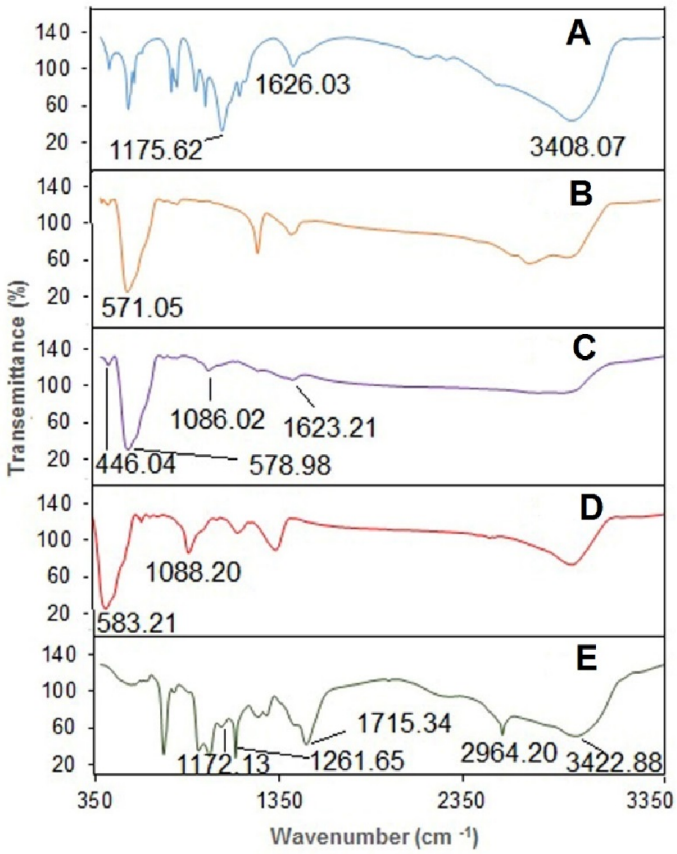

Figure 2. The FT-IR spectra of GO (A), MGO (B), MGO@IL(C), MGO@IL@AuNPs (D), and MGO@IL@AuNPs-MIP after removing DA (E).

The FT-IR spectrum of GO exhibits an absorption peak at 1175.62 cm^{-1}, which is related to the C–O bond, confirming the presence of the carboxylic group on the GO. The absorption peak in 1626.03 cm^{-1} is related to the double carbon-carbon (C=C) bond of aromatic rings and unoxidized graphite. The absorption peak in 3408.07cm^{-1} is related to hydroxyl (O–H) groups of GO (Figure 2A). The strong absorption peak in 571.05 cm^{-1} is related to the magnetic Fe-O bond (Figure 2B). The FT-IR spectrum in the 1623.21 cm^{-1} peaks is related to the tensile group of amide ($RCONR_2$). This peak proves that an amide covalent bond has been formed between the amino groups of IL and the C–H groups of GO-Fe_3O_4.

Due to the IL connection, the infrared spectrum shows peaks at 1086.02 cm^{-1} (the transformation vibration of the C–H bond of the imidazole ring), 578.98 cm^{-1} (the symmetric vibration of the C–H bond of the imidazole ring), and 446.04 cm^{-1} (in the plane vibration of the C–H bond of the imidazole ring) (Figure 2C). Furthermore, the FT-IR spectrum of GO-Fe_3O_4-IL-AuNPs exhibited absorption peaks at 583.21 $cm^{-1}$and 1088.20 cm^{-1}, which revealed the connection of AuNPs on the GO-Fe_3O_4-IL surface through covalent bonding (Figure 2D). The absorption peaks at 1172.13 cm^{-1}

and 1261.65 cm^{-1} are related to O–C–O and C–O bonds, respectively. Symmetric and asymmetric vibrations of C–H cased to the peak at 2964.20 cm^{-1}. Finally, the strong peak at 1715.34 cm^{-1} was related to the carbonyl group, and the weak peak at 3422.88 cm^{-1} was due to the O–H group after removing the template (Figure 2E).

Electrochemical characterization

Different electrochemical properties and EIS data between various modified electrodes were investigated by cyclic voltammograms (CVs) and EISspectra in a $[Fe(CN)_6^{-3/-4}]$ solution (Figure 3).

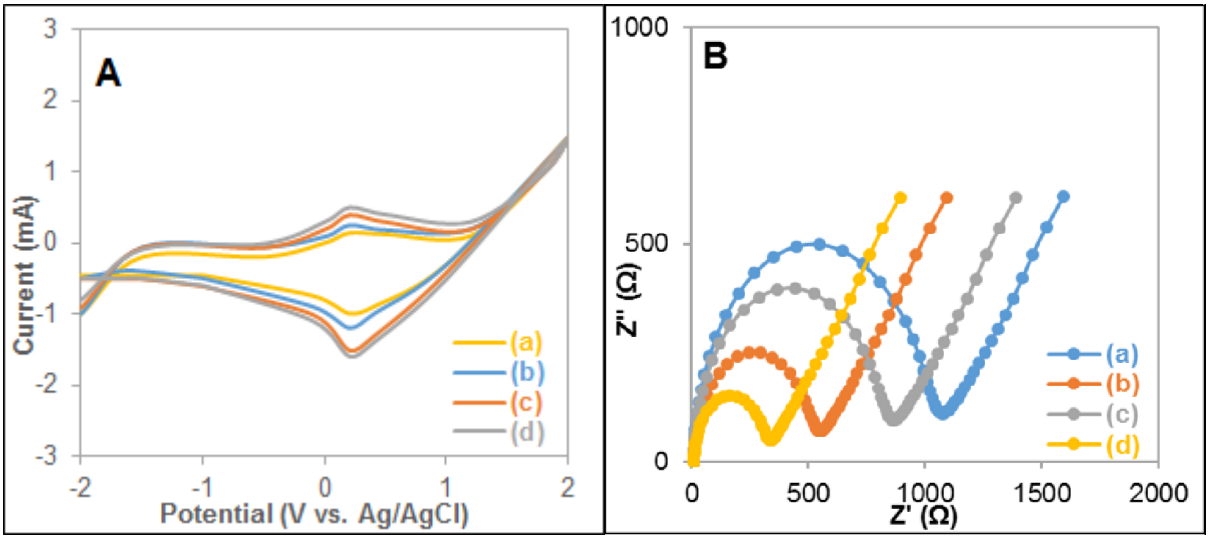

Figure 3. (A) CVs in a 0.02 M $[Fe(CN)_6^{-3/-4}]$ solution: bare graphite (a), GO (b), MGO@IL (c) and MGO@IL@AuNPs (d) electrodes. (B) Impedance spectra in a 0.02 M $[Fe(CN)_6^{-3/-4}]$ solution: bare graphite (a), MGO@IL@AuNPs (b) MGO@IL@AuNPs-MIP before removing DA (c) and MGO@IL@AuNPs-MIP after removing DA electrodes (d) (pH =7; the scan rate of 0.1 V. s^{-1}).

As shown in Figure 3A, the bare electrode (a), GO (b), GO-Fe_3O_4(c), and GO-Fe_3O_4-AuNPs (d) were investigated in a 0.02 M$[Fe(CN)_6^{-3/-4}]$ solution by a variety of CVs. The scan rate was 0.1 $V.s^{-1}$, and the scan range was between -2 to +2 V. Small anodic and cathodic peaks could be observed in the bare electrode (curve a), and the current increased in the GO electrode (curve b). After adding Fe_3O_4 particles and IL to the electrode surface, the CVs showed steady redox peaks, and the current increased (curve c).

Then, AuNPs were added and a clear increase in redox peaks was observed. The results indicated that the stability, conductibility, and electrocatalyst of the electrodes were enhanced by the modifying particles. According to Randles–Sevcik equation [19], the active surface area was calculated for bare electrode, GO, GO-Fe_3O_4-IL, and GO-Fe_3O_4-IL-AuNPs electrodes. 0.136, 0.164, 0.205, 0.219 cm^2 values were obtained from the calculations. The results showed that GO-Fe_3O_4-IL-AuNPs electrodes have high efficiency due to the provision of a large active surface area.

The impedance data could be fitted to the Randles circuit [20] as shown in Figure 3B. The impedance spectra include a semi-circular portion related to charge-transfer resistance (R_{ct}) and a linear portion related to electrolyte resistance (R_s). Figure 3B shows the curve of the bare electrode (curve a), GO-Fe_3O_4-IL-AuNPs (curve b), the curve GO-Fe_3O_4-IL-AuNPs@MIP before removing DA (curve c), and of GO-Fe_3O_4-IL-AuNPs@MIPafter removing DA (curve d) in 0.02 M [$Fe(CN)_6^{-3/-4}$] solution which indicates the Nyquist plotlines [21].

The R_{ct} for the curve of the bare electrode (curve a) was high (1000 Ω). The R_{ct} for the curve of GO-Fe_3O_4-IL-AuNPs (curve b) decreased (500 Ω), indicating that added particles are excellent electric conducting materials. The R_{ct} increased after coating GO-Fe_3O_4-IL-AuNPs@MIP (800 Ω) (curve c), indicating that the template was successfully composited on the surface. The MIP particles blocked the electron exchange between the solution and the electrode. After removing the template, R_{ct} decreased (300 Ω) (curve d), indicating that the template was successfully removed and the conductivity of the electrode was increased.

Optimizing the preparation conditions of the electrochemical sensor

Optimization of the type of supporting electrolyte

Supporting electrolytes are an important factor for accessing a quality electrochemical signal in an electrochemical sensor. Different types of supporting electrolytes such as NH_4Cl, KNO_3, KCl, and NH_4NO_3 were used in the potential range of -2 to 2 V in the CV curves in a 1×10^{-4} M DA solution. According to the results, when NH_4Cl and KCl were used, the NH_2 group in DA interacted with Cl of NH_4Cl and KCl and the color of the analysis solution changed. NH_4NO_3 as a supporting electrolyte caused a buffering system in the solution and the pH of the solution changed. The current response was excellent when the concentration of the electrolyte was increased. Therefore, the 0.1 M KNO_3 solution was selected as the optimum supporting electrolyte in the analysis solution (Figure 4).

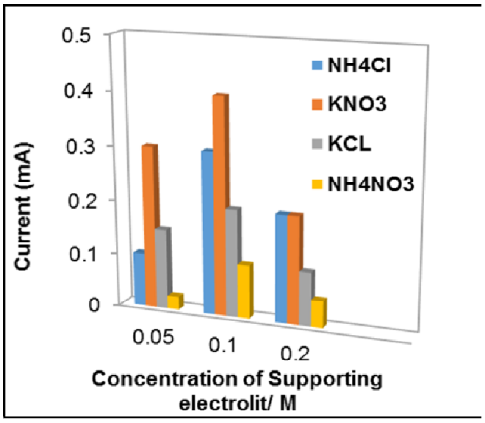

Figure 4. The effect of the type of the supporting electrolyte on the electrochemical signal (pH=7; scan rate=0.1 $V.s^{-1}$).

pH Optimization

The pH value of the solution is an important factor effect on electron transfer rate[22]. In the current work, DA solutions with pH values ranging from 2 to 8 and six different concentrations (1×10^{-5}, 2×10^{-5}, 4×10^{-5}, 6×10^{-5}, 8×10^{-5}, and 1×10^{-4} M) were prepared. Figures 5A and B showed the relation of the peak current of DA in CV and DPV. The peak current of DA increased as pH increased and showed the maximum signal at pH=7. After pH=7peak current of DA suddenly decreased. Therefore, as shown in Figures 5C and D in CV and DPV studies pH=7 was selected as the optimum pH.

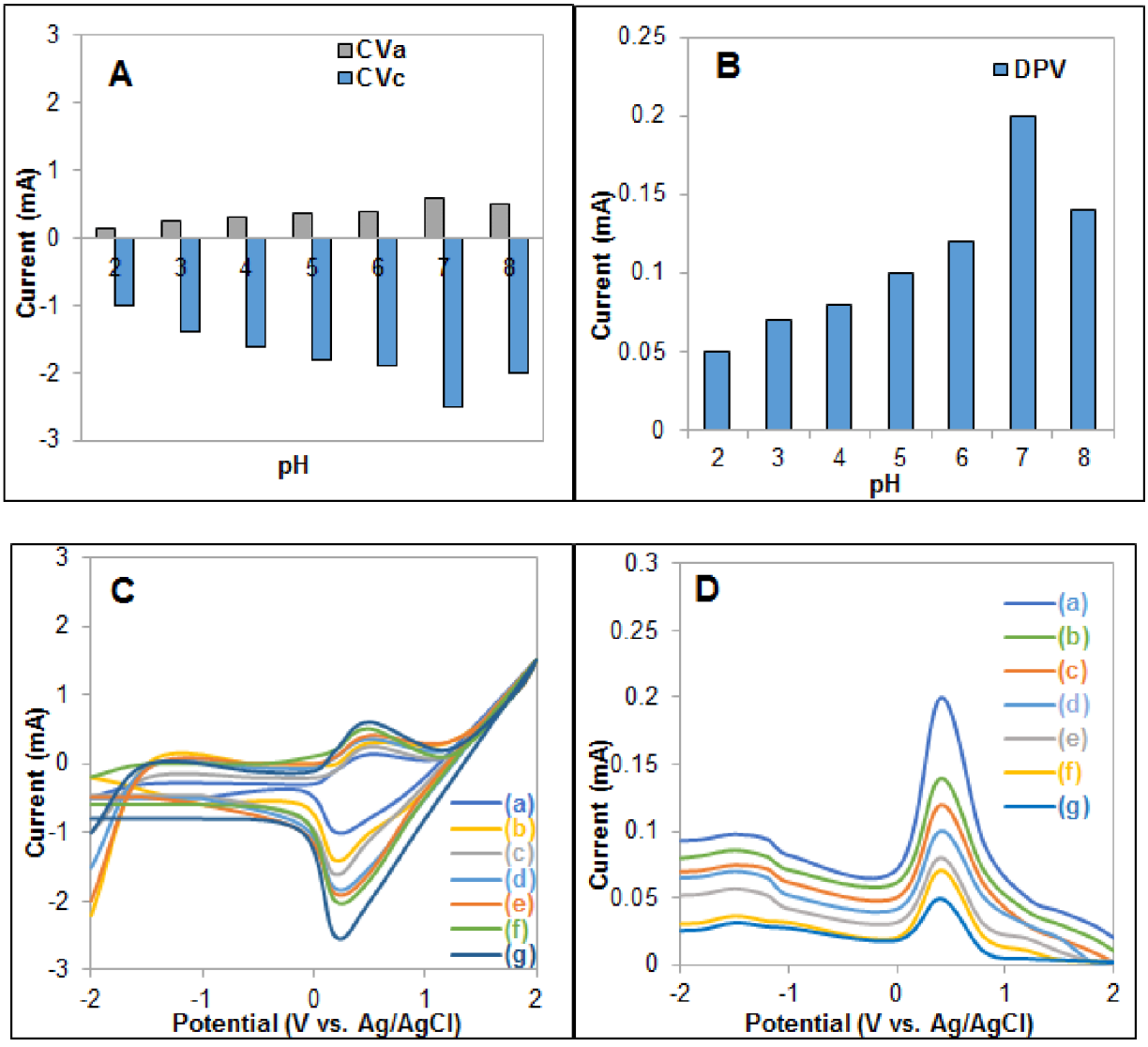

Figure 5. (A) and (B) the effect of pH on the modified electrode signal in the CVs and DPVs. (C) and (D) respectively demonstrate the CVs and DPVs of the modified electrode in the DA solution with different pHs (a, 2; b, 3; c, 4; d, 5; e, 6; f, 8; g,7); (the scan rate was 0.1 $V.s^{-1}$).

Influence of scan rate on the sensor response

The effect of the various scan rates on the peak current was investigated. Cyclic voltammograms were recorded between 0.025 to 0.1 $V.s^{-1}$ in 4×10^{-6} M DA solution at pH=7 from -2 to 2 V potential range (Figure 6A). The results in Figure 6A showed that by increasing scan rate, the anodic and cathodic peaks current of DA was increased linearly. According to Figures 6B and 6C, the redox peak current and peak potential versus scan rate (ν) and logarithm scan rate (ν) were studied respectively. The linear relationship between the redox peak currents and scan rate (ν) indicated that the scan rate (ν) was affected by the electrode process.

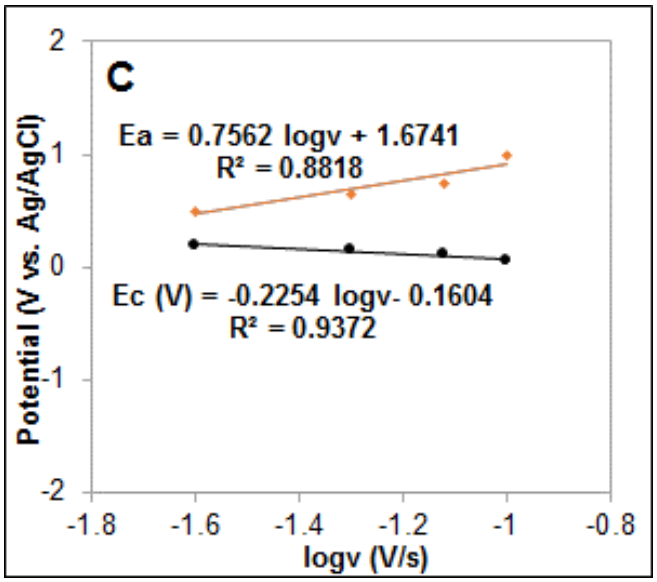

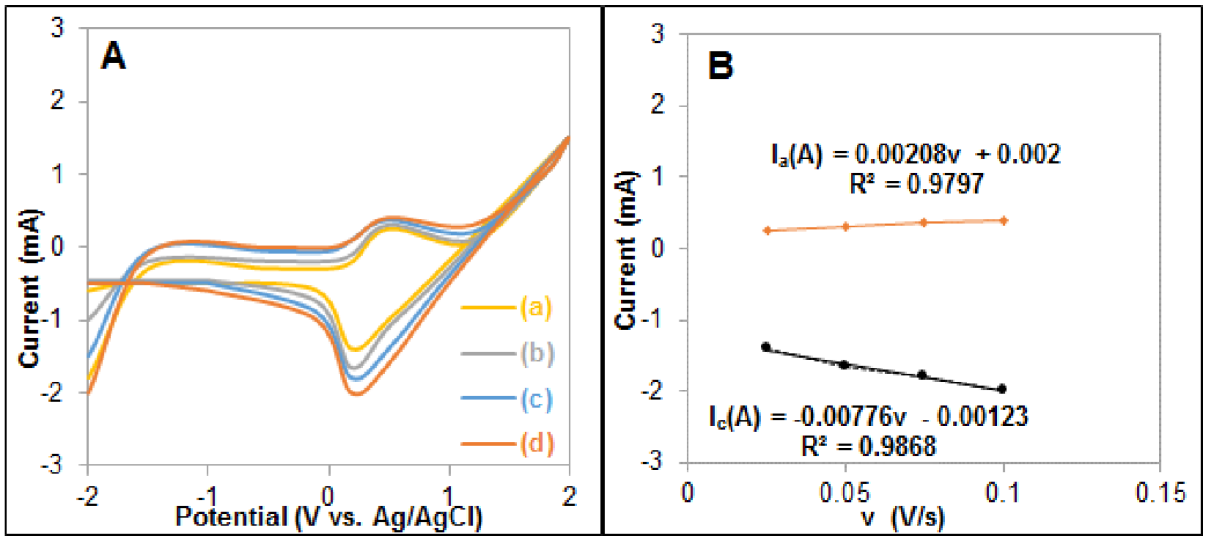

Figure 6. (A) The CVs of the 4×10^{-6} M DA solution at different scan rates of a, 0.025; b, 0.05; c, 0.075; and d, 0.1 $V.s^{-1}$ (d) (pH=7).(B) The anodic and cathodic peak currents of4×10^{-6} MDAsolution at different scan rates of 0.025, 0.05, 0.075, 0.1 $V.s^{-1}$. (C) The anodic and cathodic peak potantial of DA at different logarithm scan rates of 0.025, 0.05, 0.075, 0.1 $V.s^{-1}$.

The analytical properties of the electrochemical sensor

Calibration curve

The calibration curve of DA was investigated by DPV with high sensitivity, low detection limit, and wider concentration range (Figure 7A). Under optimal conditions, in the linear concentration range, 6×10^{-8} to 1×10^{-5} M DA correlation coefficient was 0.98. The regression equation was I(A) = 18.774 C(M)+ 0.0000905 (R^2= 0.98), and the detection limit was estimated to be 1×10^{-10} M (S/N=3) (Figure7B). As shown in Table 1, this concentration range was wider and lower than those of usual methods.

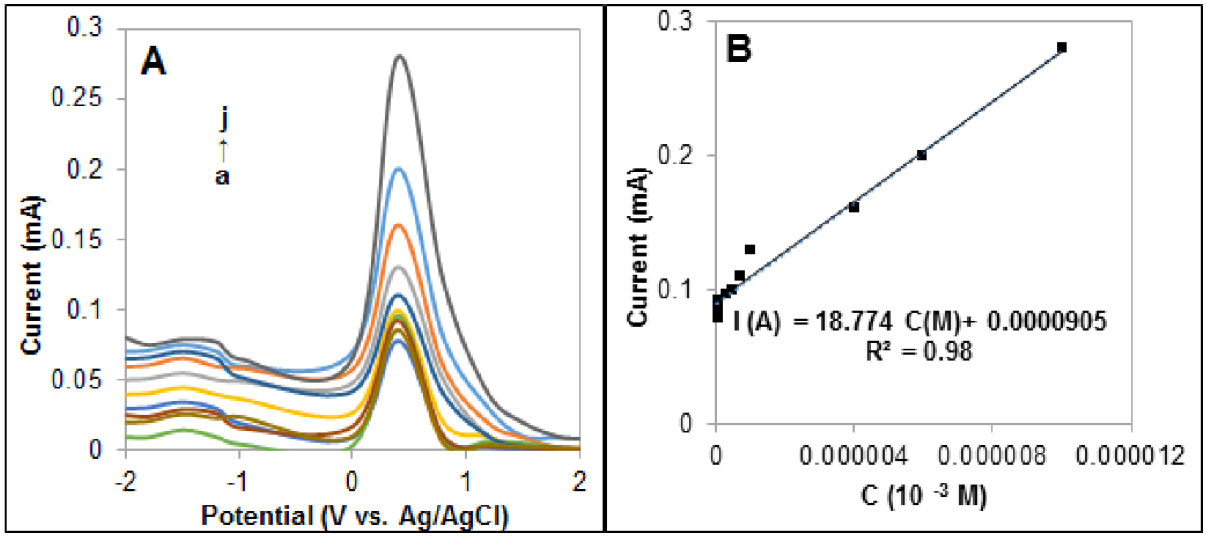

Figure 7. (A) DPVs in: 6×10^{-8}, 8×10^{-8}, 10^{-7}, 3×10^{-7}, 5×10^{-8}, 7×10^{-7}, 10^{-6}, 4×10^{-6}, 6×10^{-6}, and 10^{-5} M DA solutions (pH=7; scan rate=0.1 $V.s^{-1}$). (B) The linear relationship between the electrochemical signal and the concentration of DA (the concentrations of DA were: 6×10^{-8}, 8×10^{-8}, 10^{-7}, 3×10^{-7}, 5×10^{-8}, 7×10^{-7}, 10^{-6}, 4×10^{-6}, 6×10^{-6}, and 10^{-5} M).

Table 1. The analytical properties of different detection methods for the determination of DA.

Method	Detection limit/M	Linear range/M	Ref
MIP electrochemical sensor	1×10^{-7}	3×10^{-7} to 1×10^{-4}	[23]
A novel PVC MIP electrochemical sensor	3.7×10^{-7}	1×10^{-6} to 1×10^{-1}	[24]
Electrochemical sensor based on dual-template molecularly imprinted polymer and nanoporous gold	4×10^{-7}	0.18×10^{-8} to 2×10^{-6}	[25]
Electrochemical sensor based onnitrogen doped graphen	2.5×10^{-7}	5×10^{-7} to 1.7×10^{-4}	[26]
MGO-IL-Au NPs-MIP	1×10^{-10}	6×10^{-8} to 1×10^{-5}	Present work

Sensor selectivity

The selectivity of the MIP sensor was investigated by the solution containing 3×10^{-7} M DA, uric acid (UA), and ascorbic acid (AA). UA and AA were used as the interferential compounds. The results indicated that 50-fold of UA and AA did not affect of DA signal. Moreover, the 100-fold concentration of Na^{+}, Mg^{2+}, Al^{3+}, NO^{3-}, SO_4^{2-} ions did not influence the current of DA. The results showed that the current response of the MIP sensor for DA was much higher than other compounds, indicating the cavities of MIP were well-fitted with the DA structure and cannot bind to other structures (Figure 8).

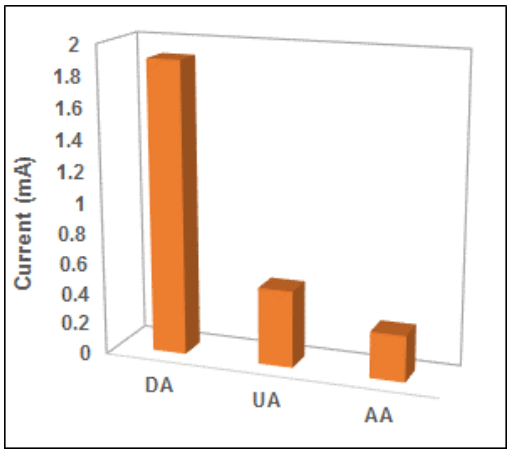

Figure 8. The selectivity of the MIP sensor for DA and the interferences.

Measuring DA in real samples

To investigate the performance of the designed sensor in DA detection standard addition procedure was used. In this way, blood serum and urine samples were prepared using 25 mL $Ba(OH)_2$ (1 wt%) and 25 mL $ZnSO_4$. The MIP sensor had selectivity toward the DA template molecules. The recovery percentage and RSD of the sensor are presented in Table 2. Good measurement accuracy was obtained and the recovery range was 98%>. These results suggest that the proposed method can be used to analyze DA in real samples.

Table 2. The determination of DA in real samples (n=3).

Samples (7×10^{-7} M)	Added (7×10^{-7} M)	Found (7×10^{-7} M)	Recovery (%)	RSD (%)
	7.2×10^{-7}	8×10^{-7}	100>	2.2
Urine	1.01×10^{-7}	1×10^{-7}	99	1.4
	3.06×10^{-7}	3×10^{-7}	98	1.7
	5.05×10^{-7}	5×10^{-7}	99	1.1
Blood	7×10^{-7}	7.1×10^{-7}	100>	2.1
	1.01×10^{-6}	1×10^{-6}	99	1.3

Conclusions

In this paper, Fe_3O_4 was used to increase the current signal of the electrochemical sensor.IL was successfully grafted on the surface of GO-Fe_3O_4 and was used as a supporting material to graft MIP on GO-Fe_3O_4. AuNPs were coated on the surface of GO-Fe_3O_4-ILand improved the conductivity of this electrochemical sensor. The modified MIP sensor was applied for the detection of DA in real samples with satisfying results. This work provided a useful platform for the preparation of a MIP sensor based on GO-Fe_3O_4modified nanocomposite.

Acknowledgments

Islamic Azad University, Tabriz Branch, Faculty of Science, and Laboratory of Chemistry supported this work.

References

[1] C.F. Valenzuela, M.P. Puglia, S. Zucca, *Alcohol Res Health*, 34, 106 (2011).

[2] A. Schatton, J. Agoro, J. Mardink, G. Leboulle, C. Scharff, *BMC Neuroscience*, 19, 69 (2018).

[3] E. Casal, L. Palomo, D. Cabrera, J.M. Falcon-Perez, *Front Pharmacol*, 7, 501 (2016).

[4] J. Chen, Y.-P. Shi, J.-Y. Liu, *J. Chromatogr. A*, 1003, 127 (2003).

[5] S. Karayaka, D.S. Chormey, M. Fırat, S. Bakırdere, *Chemosphere*, 235, 205 (2019).

[6] S.M. Banihashemian, V. Periasamy, G. Boon Tong, S. Abdul Rahman, *PLoS One*, 11, e0149488 (2016).

[7] M. Gholivand, M. Torkashvand, *Mater. Sci. Eng. C*, 59, 594 (2016).

[8] S. Akbari, S. Jahani, M.M. Foroughi, H.H. Nadiki, *J. Appl. Chem. Res.*, 14, 8 (2021).

[9] M.A. Abu-Dalo, N.S. Nassory, N.I. Abdulla, I.R. Al-Mheidat, *J. Electroanal. Chem.*, 751, 75 (2015).

[10] A. Poma, A.P. Turner, S.A. Piletsky, *Trends Biotechnol.*, 28, 629 (2010).

[11] K. Hemmati, A. Masoumi, M. Ghaemy, *Carbohydr. Polym.*, 136, 630 (2016).

[12] G. Yang, F. Zhao, *Electrochim. Acta*, 174, 33 (2015).

[13] J. Li, X. Lin, *Sens. Actuators B Chem.*, 126, 527 (2007).

[14] X. Tan, Q. Hu, J. Wu, X. Li, P. Li, H. Yu, X. Li, F. Lei, *Sens. Actuators B Chem.*, 220, 216 (2015).

[15] H.K. Kaya, S. Cinar, G. Altundal, Y. Bayramlı, C. Unaleroglu, F. Kuralay, *Sens. Actuators B Chem.*, 346, 130425 (2021).

[16] X. Ma, F. Gao, R. Dai, G. Liu, Y. Zhang, L. Lu, Y. Yu, *Anal. Methods*, 12, 1845 (2020).

[17] W. Zhao, Y. Ma, J. Ye, *J. Electroanal. Chem.*, 888, 115215 (2021).

[18] L. Shahriary, A.A. Athawale, *Int. J. Renew. Energy Environ. Eng*, 2, 58 (2014).

[19] A. García-Miranda Ferrari, C.W. Foster, P.J. Kelly, D.A. Brownson, C.E. Banks, *Biosensors*, 8, 53 (2018).

[20] Y. Xu, C. Li, W. Mei, M. Guo, Y. Yang, *Med Biol Eng Comput.*, 57, 1515 (2019).

[21] R. Pourghobadi, M.R. Baezzat, *Anal. Bioanal. Chem*, 4, 261 (2017).

[22] A. Shaikh, J. Firdaws, S.S. Badrunnessa, M. Rahman, P.K. Bakshi, *Int J Electrochem Sci*, 6, 2333 (2011).

[23] J. Yang, Y. Hu, Y. Li, *Biosens. Bioelectron.*, 135, 224 (2019).

[24] N. Dere, Z. Yolcu, M. Yolcu, *Acta Chim Slov.*, 15, 69(1), 108 (2022).

[25] N. Li, C. Nan, X. Mei, Y. Sun, H. Feng, Y. Li, *Microchim Acta*, 187, 1 (2020).

[26] Z.-H. Sheng, X.-Q. Zheng, J.-Y. Xu, W.-J. Bao, F.-B. Wang, X.-H. Xia, *Biosens. Bioelectron.*, 34, 125 (2012).